International Journal of Electrical and Computer Engineering (IJECE)
Vol. 13, No. 4, August 2023, pp. 3695~3705
ISSN: 2088-8708, DOI: 10.11591/ijece.v13i4.pp3695-3705

Numerical analysis in $Ar\text{-}H_2$ coupled-coil inductively coupled thermal plasma with Si feedstock for stable operation

Yulianta Siregar[1], Yasunori Tanaka[2]
[1]Department of Electrical Engineering, Universitas Sumatera Utara, Medan, Indonesia
[2]Faculty of Electrical Engineering and Computer Science, Kanazawa University, Kanazawa, Japan

Article Info

Article history:

Received Sep 20, 2022
Revised Dec 12, 2022
Accepted Dec 17, 2022

Keywords:

Ar-H2
Coupled coil
Inductively coupled thermal plasma
Nanoparticle synthesis

ABSTRACT

In nanopowder synthesis, the starting powder to be evaporated is infused in a plasma torch through the upper coil and the lower coil in the coupled model of inductively coupled thermal plasma (coupled-coil inductively coupled thermal plasma (ICTP)). Mixing these evaporated materials to form the coupled ICTP significantly influences the thermodynamic and transport properties. It is essential to understand these complex interactions between coupled ICTP and feedstock evaporation. This research investigated the thermal interactions between silicon raw material powder (Si) with ICTP in coupled 99%Ar/1%H2 through the numerical model developed for the synthesis of Si nanopowder. The feed rate of the Si raw material was set at 0.05, 0.1, and 0.5 g/min. This implies that the increased Si feed is too heavy to vaporize all the injected feed.

This is an open access article under the CC BY-SA license.

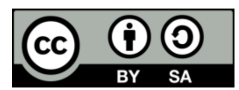

Corresponding Author:

Yulianta Siregar
Department of Electrical Engineering, Faculty of Engineering, Universitas Sumatera Utara
St. Dr. T. Mansur No. 9, Medan City, Sumatera Utara Province, Indonesia
Email: julianta_srg@usu.ac.id

1. INTRODUCTION

Inductively coupled thermal plasma (ICTP) at high power and high pressure is commonly used as a heat resource and a chemical resource in material handling. Examples are thermal barrier spray coating [1], [2], transparent conductive oxide deposition [3], diamond film deposition [4], [5], and surface transformation [6]. The advantage of ICTP in preparing this material is that ICTP has a high density and high enthalpy of chemical species with a gas temperature of about 10,000 K. In addition, ICTP does not require electrode removal. It can offer clean thermal plasma without any contamination measure for this benefit. The synthesis of nanomaterials is one of the important applications of ICTP, such as nanotubes [7], [8], nanoparticles [9]–[14], fullerenes [15], [16]. In these examples, the ICTP process is generally used by a one coil ICTP close to the plasma torch.

Synthesis of nanomaterials in plasma torch, the raw material powder is infusion to be evaporated in ICTP with the high-temperature field. Mix this evaporated material into the cooled ICTP to nucleate and synthesize the nanomaterials. Meanwhile, its effect on the thermodynamic properties and the main plasma transport properties causes changes in temperature and gas flow field and the evaporation rate of raw materials at ICTP. During this treatment, ICTP has a large infusion of raw material powder and causes instability with disruptive effects. In surprising cases, ICTP can be restrained by too heavy an infusion of raw material powder.

The solution to this problem, a coupled coil model of inductively coupled thermal plasma (coupled coil-ICTP), has been developed. The coupled coil-ICTP has two different coils in a dielectric cylindrical tube. Research conducted by Siregar *et al.* [17] on coupled coil-ICTP for injecting raw material powder and

plasma torch. Several numerical studies have also studied temperature behaviour in coupled coil-ICTP [17]–[19]. We also expanded the coupled type of pulse-induction modulated thermal plasma system (coupled-PMITP) [20] and later the coupled-ICTP system. The currents of the two amplitude-modulated coils provided by the two different input powers are suitable for coupled-PMITP. It can produce temporally and spatially modulated induced thermal plasma fields. It can produce transiently and spatially modulated induced thermal plasma fields, which can be used for advanced material processing. However, several publications have been published on the temperature field and gas flow in the linked coil-ICTP with increasing raw material powder infusion.

The main objective of this work is a computational program that was used in a coupled coil ICTP with powder infusion analysis to find the gas flow field and temperature behaviour by regenerating our calculation type for a one-coil ICTP with powder infusion of matter [21]–[24]. The Inductively coupled thermal plasma (ICTP) coupled-coil is suitable for upper and lower coils of the same diameter. The two disjunct coil currents (upper and lower coils) in the coupled coil ICTP are provided by two different interrupted input current resources with different running frequencies. While the powder of the infusion feedstock evaporates in the lower coil area of the ICTP, the upper coil's maximum temperature area can be used to stabilize the ICTP.

This coupled-coil ICTP could be useful, for example, for the synthesis of nanomaterials. The advanced type for coupled-coil ICTP with the infusion feedstock powder solves the energy, momentum, and mass conservation calculation for thermal plasmas involving thermal interactions with the infusion feedstock powder. The motion of the powder particles is obtained by solving the computational equations for the individual particles. The effect of infusion rate on gas flow field and temperature was investigated. This investigation found a specific allocation for the starting material vapor concentration and temperature in the coupled-coil ICTP.

2. THE PROPOSED METHOD

The coupled coil-ICTP configuration has two types with different turn numbers in one plasma torch. ICTP torch configuration with eight-turn and twelve-turn coils, as shown in the Figures 1(a) and (b), respectively, for the coupled-coil plasma torch [20]. The plasma torch is constructed of an inner diameter of 64 mm, and a quartz tube with a length of 320 mm. Running water cooled by water sits on the walls of the quartz tube. This torch has a topmost coil and bottom coil in one plasma torch for the coupled coil. The length of each coil is 20 mm. The distance between the ends of the topmost coil and the topmost of the bottom coil is set at 40 mm for all conditions. In this paper, the infusion feeding powder is set to three feed rates such as 0.05, 0.1, and 0.5 g/min for calculation. The one-coil has 8 swivel coils with one plasma torch and is connected to one power resource at the operating frequency [21]. In this study, an electromagnetic field is produced at one frequency. Two main conditions are considered for coupled coils: One situation has 8 rotating coils. The other has 12 swivel coils with two disjunct coils in single plasma torch. It is connected to two separate power sources at different frequencies. In this study, the frequency of the electromagnetic field produced is split into two components. In this case, we have assumed two coils to relate to two different rated 450 and 300 kHz are the two most common frequencies on two different RF powder supplies of 15 and 10 kW to give the rf coil current. Our experiment discusses different operating frequencies with a decoupling electrical circuit for each coil [22].

Meanwhile, a combination of argon (Ar) and hydrogen (H_2) gas is produced as the envelope gas from the topmost of the plasma torch. To prevent plasma from entering the quartz tube, sheath gas is given along the inner wall of the tube with a vortex. The electromagnetic field produced by the connected coil's current can hasten the electrons in the plasma of the torch to produce plasma mainly by the effect of electron ionization. A water-cooled line for powder infusion of raw materials is attached from the top of the torch to the lower coil's 4-5 turns coil along the middle axis, as depicted in Figures 1(a) and (b). In the case of the synthesis of Si nanomaterials, Silicon (Si) feedstock powder is infused from above through the torch axis concurrently with carrier gases Ar and H_2 by water-cooled pipes [21], [23].

This paper makes numerical calculations to simulate the gas flow field and temperature. The coupled coil-ICTP described above operates at two different frequencies. Furthermore, in our research, one-coil ICTPs are operated with one frequency, and coupled ICTPs at two frequencies are simulated numerically. The one-coil ICTP was treated as an infusion of feeding powder at 0.05, 0.1, and 0.5 g/min between two coils with the same operating frequency. On the other hand, coupled ICTP has the same infusion powder as one coil ICTP between two coils with the same operating frequency and two different operating frequencies [25].

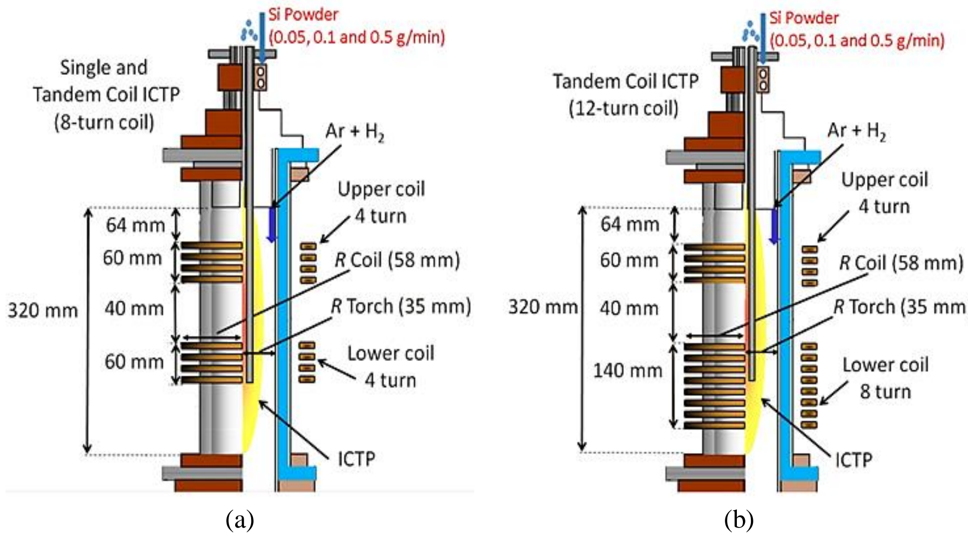

(a) (b)

Figure 1. Structure ICTP torch has two coils (a) an eight-turn coil and (b) a twelve-turn coil

3. METHOD

3.1. Modelling assumptions of coupled-coil ICTP

The ICTP coupled coil design is based on the basic particle-source-in-cell (PSI-cell) research from Crowe *et al.* [26]; this method is in addition to Proulx *et al.* trials [27], [28]. The design implies that the following situations adjust to the coupled coil ICTP: i) The ICTP coupled coil is in thermodynamic equilibrium on a local level (LTE). As a result, all temperatures are the same, including the electron temperature, excitation temperature, and severe particle temperature. The chemical equilibrium situation is confirmed in advance for all reactions; ii) Optical thinning is approximate for plasmas at wavelengths bigger than 200 nm. For wavelengths smaller than 200 nm, 20% of the amount emission coefficient is calculated to examine the successful light absorption for radiation displacement [29], [30]; iii) Laminar, axisymmetric and stable flow is estimated with negligible viscous dissipation; iv) Particle-to-particle connection is not required for the infusion resource material particles; v) The raw material powder radius is significantly bigger than the plasma fraction's mean free path; vi) The starting powder is always spherical, even during evaporation; vii) The powder surface of the raw material is warming evenly by the surrounding thermal plasma. As a result, uniform evaporation also occurs around the surface of the particle; viii) The influence of the particle's electrical charge is not critical; ix) The missile's impact by the emitted ablation steam is not significant; and x) Infusion of titanium raw material powder is evaporated individually by thermal plasma heat. Therefore, evaporation develops uniformly about the particle surface [31].

3.2. Calculation conditions in one-coil ICTP and coupled-coil ICTP

As noted above, two main conditions have been considered: one situation is where two disjunct coils in a thermal plasma torch have been joined in series with the input mains power resource at a one performance frequency. The producing electromagnetic field is created at one frequency. This situation is called in this work "one frequency coil." Another situation is that the two disjunct coils in the plasma torch are joined to two exempt electrical input power resources at distinct frequencies. In this study, the resultant electromagnetic field has two units of the frequency. This state is known as "coupled coil" to describe this work.

In this numerical simulation, the topmost coil drive frequency is set at 450 kHz, and the bottom coil current is set at 300 kHz for the coupled coil ICTP. In general, the total input power of the coupled coil is 25 kW. It consists of a 15 kW topmost coil and a 10 kW bottom coil for all situations. However, the input power and one-coil ICTP frequency are 25 kW and 450 kHz, respectively. The pressure in the chamber is arranged at 300 Torr (=40 kPa). The numerical situation is described in Table 1. The Ar and OH gas compound's flow value used as the envelope gas has been set at 90 lpm and 10 lpm, respectively. The silicon feedstock powder is thought to be fed through a water-cooled tube, including into the torch shaft of the plasma torch head. For comparison, the infusion rate of Si raw material powder was set at 0.05, 0.1, and 0.05 g/min for one-coil ICTP and coupled coil ICTP. Table 2 summarizes the thermodynamic properties of the silicon starting powders used for the numerical simulations.

Table 1. Numerical analysis conditions

Parameter	Single-coil (8-turn coil)	Tandem coil (8 and 12-turn coils)
Input power [kW]	25	
- Upper coil		15
- Lower coil		10
Frequency [kHz]	450	
- Upper coil		450
- Lower coil		300
Sheath gas flow rate [L/min]	90	90
Feeding powder rate [L/min]	0.1	0.1
Carrier gas flow rate [L/min]	4	4
Pressure [Torr]	300	300

Table 2. Thermodynamic parameter of silicon

Parameter	Condition
Injection load [g/min]	0.05, 0.2, 0.5
Mass density [kg/m3]	2,329
Melting temperature [K]	1,687
Boiling temperature [K]	2,628
Latent heat for melting [J/kg]	1,787,000
Latent heat of evaporation [J/kg]	12,784,000
Specific heat of solid [J/(kg K)]	712
Specific heat of liquid [J/(kg K)]	915
Thermal conductivity [W/(m K)]	150

4. RESULTS AND DISCUSSION

4.1. Temperature allocation of one-coil ICTP

The initial calculation was carried out for one-coil ICTP Ar-H_2 with powder infusion of raw material Si to compare with the ICTP coupled coil. A one-coil has a coil that operates with the same frequency of 450 kHz and current. The ICTP's total input electrical power was arranged at 25 kW in this study. The temperature allocation of one ICTP with powder infusion at 0.05, 0.1, and 0.5 g/min is shown in Figures 2(a) to (c). As shown in Figures 2(a) to (c), the one-coil ICTP has a temperature range above 12,500 K for 10 mm <r<32 mm radial position and 140 mm <z<265 mm axial position. Current through the thermal plasma to be warming in a large temperature range. These results indicate that the low-temperature zone above expands in the axial direction with an increasing infusion of Si raw material because the energy consumption for Si raw material is evaporation.

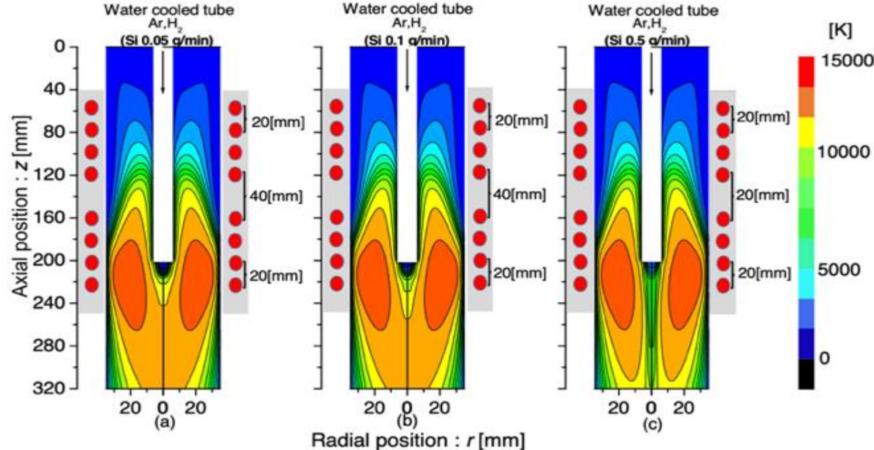

Figure 2. Temperature allocation in Ar-H_2 one-coil ICTP with Si infusion at distinct feed powder rate in (a) 0.05, (b) 0.01, and (c) 0.5 g/min

The allocation of the one ICTP temperature with increasing infusion feed rate is clearer in Figure 3. Figure 3 describes the axial temperature allocation at r=5 mm for distinct infusion feed rates. This figure shows that the temperature has the same profile on the torch axis for all conditions from z=0 mm to 220 mm.

Subsequently, this axial temperature increased by about 10,000 K (Si 0.5 g/min), 10 500 K (Si 0.1 g/min and 0.05 g/min) from z=220 mm to 280 mm.

The radial temperature allocation at z=260 mm is seen in Figure 4. As illustrated here, improving the feed rate shrinkages the axial temperature of the ICTP. However, the powder level of the raw material hardly affects the temperature beyond the 6 mm radial position. This implies that the Si administration of 0.5 g/min is too heavy to vaporize all the feedstock injected in a one ICTP. The high-temperature area uses joule heating, the more internal input power to the local one-coil ICTP. The power density allocation is shown in Figure 5 for different infusions of raw material powder, such as in Figure 5(a) 0.05 g/min, 0.01 g/min in Figure 5(b), and 0.5 g/min in Figure 5(b). This figure shows that the increase in feedstock powder infusion does not differ significantly in power density because feedstock powder infusion disrupts the high-temperature area in the one-coil just slightly.

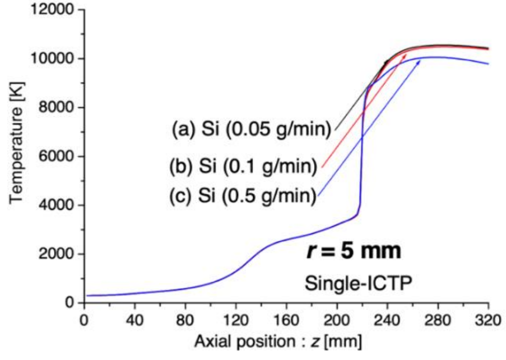

Figure 3. Axial temperature allocation in Ar-H_2 one-coil ICTP at a radial condition of 5 mm with Si infusion at distinct feed powder rate

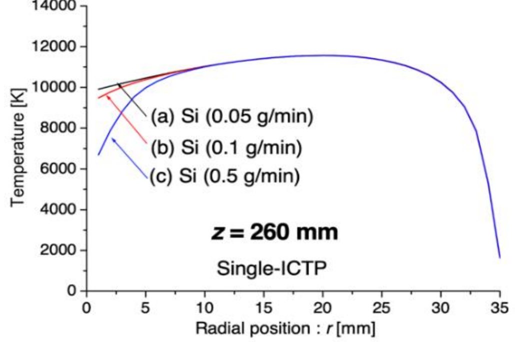

Figure 4. Radial temperature allocation at radial condition of 260 mm in Ar-H_2 one-coil ICTP with Si infusion at distinct feed powder rate

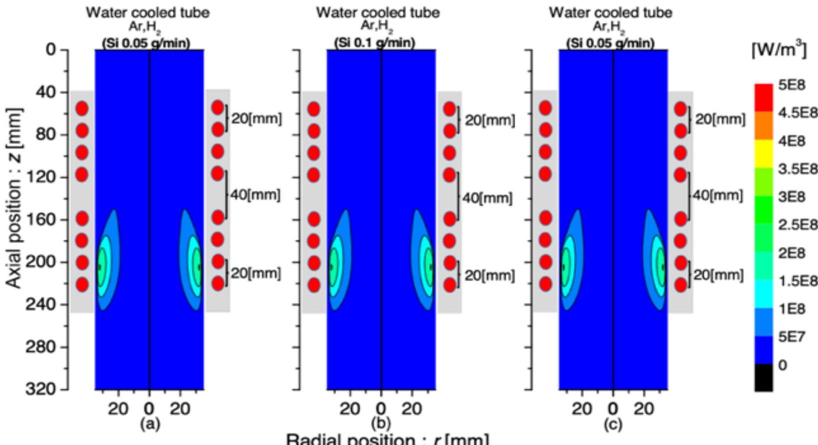

Figure 5. ArH$_2$ one-coil ICTP power density allocation through an 8 turn coil infused with Si at a given powder feed rate in (a) 0.05 g/min, (b) 0.01 g/min, and (c) 0.5 g/min

4.2. Temperature allocation of coupled-coil ICTP with eight-turns coil

A one ICTP does not have a disjunct high-temperature area, but only one high-temperature area is obtained. This chapter explains that two coupled coils are used with various frequencies of operation. The temperature allocation in a coupled-coil ICTP with eight turns, with powder infusion of 0.05, 0.1, and 0.5 g/min powder as shown in Figures 6(a) to (c), respectively. This numerical simulation incorporates the fixed input electrical power of the upper and lower coils to 10 and 15 kW, respectively. Figures 6(a) to (c) show that the temperature allocation has elongated agglomerate in the high-temperature zone. This high-temperature area lowers the axial temperature by increasing the infusion of raw material powder between coils from 0.05 to 0.5 g/min. Current flow in the thermal plasma to be warming in high-

temperature areas. These results indicate that with an increasing infusion of Si raw material, the axial temperature shrinkages because the energy consumption for Si raw material is evaporation. Furthermore, coupled-ICTP with eight coil windings reaches a maximum temperature of about 15,000 K, higher than one-coil ICTP.

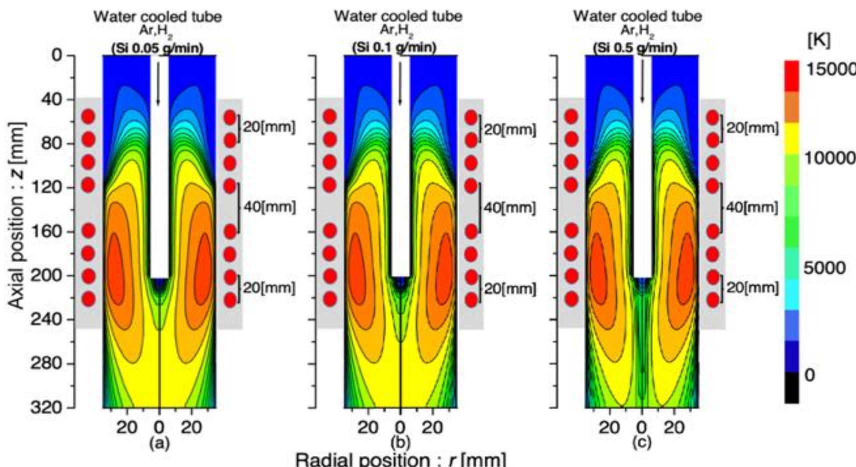

Figure 6. Temperature allocation in Ar-H2 coupled-coil ICTP using an 8-turn coil and Si infusion at a distinct feed powder rate in (a) 0.05, (b) 0.01, and (c) 0.5 g/min

Figures 7 and 8 depict the axial temperature distribution at r=5 mm and the radial temperature distribution at z=260 mm, respectively, to explain the temperature difference in the powder infusion conditions of raw materials. As shown in Figure 7, the axial temperature in the ICTP coupled coil (8 coils) is almost the same as in Figure 3. The temperature does not change on the torch axis for all conditions from z=0 mm to 220 mm. Subsequently, this axial temperature increased by about 10,000 K (Si 0.5 g/min), 10 and 500 K (Si 0.1 and 0.05 g/min) from z=220 to 280 mm.

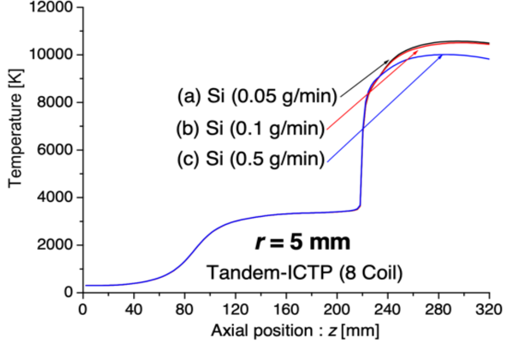

Figure 7. Axial temperature allocation in Ar-H_2 coupled-coil ICTP using a radial condition of 5 mm and Si powder infusion at a distinct feed powder rate

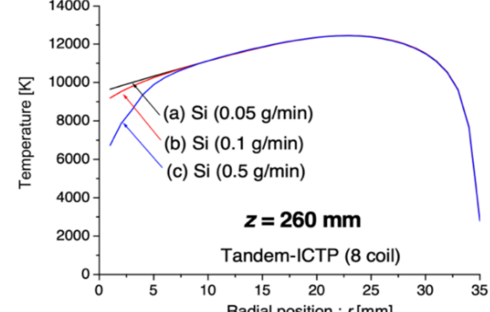

Figure 8. Radial temperature allocation at radial condition of 260 mm in Ar-H_2 coupled-coil ICTP with Si powder infusion at distinct feed powder rate

The temperature allocation of the eight-winding ICTP coupled-coil radial in Figure 8 is slightly different from that of the one ICTP in Figure 4. The coupled coil ICTP at a temperature allocation of z=260 mm reaches a maximum temperature of about 12,500 K, higher than that of the one coil ICTP. As depicted in Figure 8, increasing the feed rate lowers the axial temperature of the coupled-coil ICTP. However, the powder infusion of raw materials hardly affects the temperature outside of the 7 mm radial position. This implies that administering Si at 0.5 g/min is too heavy to vaporize all the feedstock injected in the coupled-coil ICTP with eight coil turns.

The high input power of the joule heating is shown in Figure 9. The power density allocation of joules heating in a coupled-coil ICTP torch with 8-turns is depicted in Figures 9 (a) to (c) with powder feed rate in 0.05 g/min, 0.01 g/min, and 0.5 g/min. As shown there, the increase in feedstock powder infusion did not differ significantly in power density because feedstock powder infusion only marginally interrupted the high-temperature zone in the higher coil. The bottom coil's large temperature area can also be employed to evaporate the powder infusion.

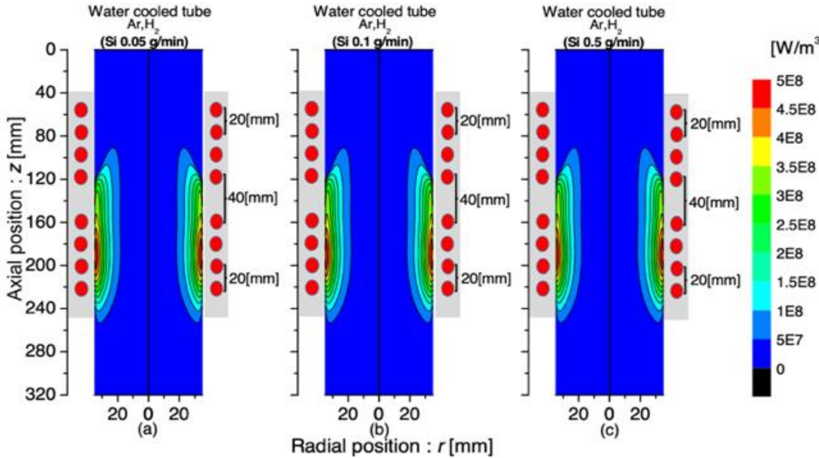

Figure 9. Ar-H_2 coupled-coil ICTP power density allocation through an 8 turn coil infused with Si powder at a given powder feed rate in (a) 0.05 g/min, (b) 0.01 g/min, and (c) 0.5 g/min

4.3. Temperature allocation of coupled-coil ICTP with twelve-turns coil

Temperature allocation in a coupled ICTP with 12 rotating coils on different feeding powder infusions of 0.05, 0.1, and 0.5 g/min, as depicted in Figures 10(a) to (c). The water-cooled pipe is set to z=220 mm in this case. The temperature allocation on the 12-turn coil in Figure 10 is longer, from z=105 mm to z=220 mm, than the temperature allocation on the 8-turn coil in Figure 6, but the maximum temperature is lower. This high-temperature area lowers the axial temperature by increasing the infusion of raw material powder between coils from 0.05 to 0.5 g/min. Current flow in the thermal plasma to be warming in high-temperature areas. These results indicate that the above low-temperature area extends in the axial direction with an increasing infusion of Si raw material. The energy consumption for the Si raw material is coupled-evaporating ICTP with a twelve-turn coil. Furthermore, the ICTP coupled coil with twelve turns reaches a maximum temperature of about 14,000 K, less than the ICTP coupled with eight turns.

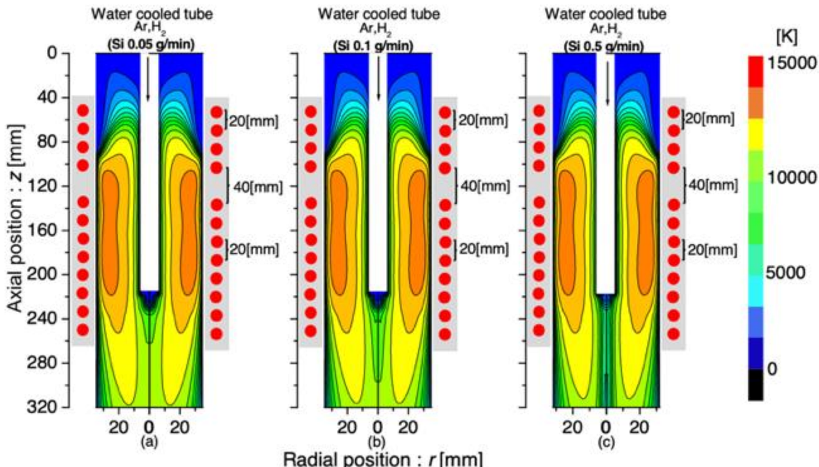

Figure 10. Temperature allocation in Ar-H_2 coupled-coil ICTP using a 12-turn coil and Si infusion at a distinct feed powder rate in (a) 0.05, (b) 0.01, and (c) 0.5 g/min

The axial temperature allocation at r=5 mm in the coupled-coil ICTP (12 coils) with different feedstock powder infusions is depicted in Figure 11. As provide in Figure 11, the axial temperature in the ICTP coupled coil (12 coils) is almost the same as in Figures 3 and 7. The temperature did not change on the torch axis for all conditions from z=0 to 220 mm, but the lowest maximum temperature allocation was at feed rates of 0.5, 0.1, and 0.05 g/min.

The radial temperature allocation of the coupled-ICTP with twelve windings in Figure 12 is slightly different from that of the one ICTP in Figure 4 and the coupled coil (8 coils) in Figure 8. As depicted in Figure 12, an increase in the feed rate shrinkages the axial temperature of the coupled-ICTP. However, the powder infusion of raw materials hardly affects the temperature beyond the radial position of 7.5 mm. This implies that the Si administration of 0.5 g/min is too heavy to vaporize all the co-injected feedstock-ICTP with twelve coil turns. Furthermore, the temperature allocation reaches a maximum temperature of about 11,500 K, which is smaller than coupled-ICTPs with eight coil windings.

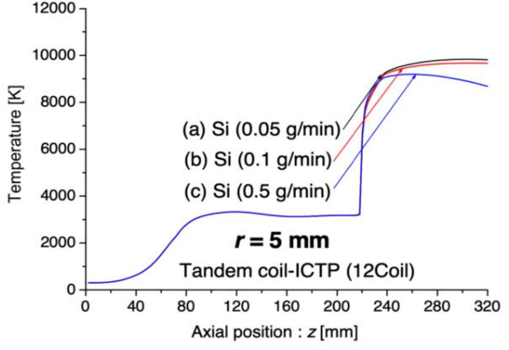

Figure 11. Axial temperature allocation in Ar-H_2 coupled-coil ICTP using a 12-turn coil and Si infusion at different feed powder rates at a radial condition of 5 mm

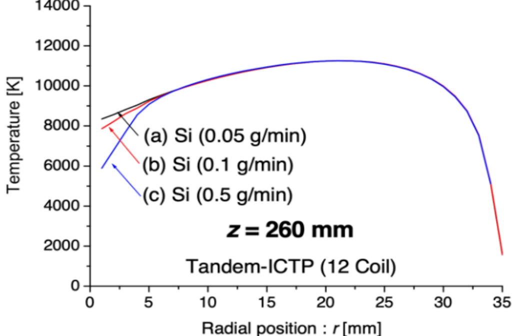

Figure 12. Radial temperature allocation in Ar-H_2 coupled-coil ICTP using a 12-turn coil and Si infusion at distinct feed powder rate at the radial condition of 260 mm

The power density of a coupled ICTP with a coil of 12 windings with Joule heating is also shown in Figure 13 with powder feed rate in (a) 0.05 g/min, (b) 0.01 g/min, and (c) 0.5 g/min. The configuration and combination of the coupled-ICTP can affect the temperature allocation and the allocation of the input power density. The comparison of the high-power density zone with coupled-ICTP (12 coils) is located higher up, as depicted in Figure 13, although the coupled-coil ICTP (8 coils) is positioned downwards. In this way, the high-temperature area and the input power density can be controlled by adopting a coil configuration.

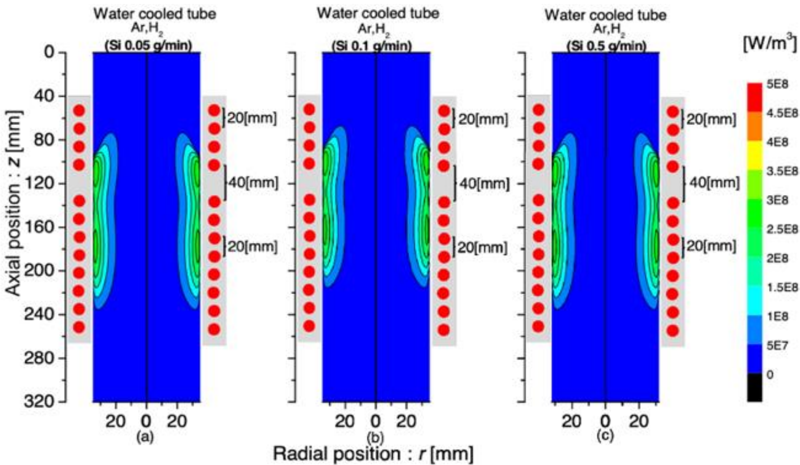

Figure 13. Ar-H_2 coupled-coil ICTP power density allocation through a 12 turn coil infused with Si powder at a given powder feed rate in (a) 0.05 g/min, (b) 0.01 g/min, and (c) 0.5 g/min

The behavior of the Si raw material particles injected into the ICTP one-coil and the ICTP coupled should be estimated with the particles warming, melting, and evaporating because of their mobility. Furthermore, the decrease of particle diameter across time and space during the evaporation procedure. Figure 14 shows the variation in particle diameter as a purpose of axial location in a one ICTP with 0.5 g/min powder infusion of the starting material. The behavior of 35 particles was the count for the 7 diameters and 5 starting locations of the infusion particles for statistical studies. Figure 14 described that the particle diameter does not require replacement to 220 mm in the axial location because the particles are all contained within the water-cooled pipe. The particles began to fly towards the ICTP from a 220 mm axial point. ICTP then heats it up. After heating during its flight, evaporation causes the diameter of the Si powder to shrink. The particle diameter gradually shrinks to 0.25 m while the ICTP warms the particles violently, which leads to the formation of Si vapor in the ICTP. As seen this illustration, all particles evaporate completely in seven initial locations with five initial diameters up to an axial location of 265 mm.

Figure 15 shows the fluctuation of Ti particle diameter in an ICTP coupled coil with an eight-turn coil with 0.1 g/min powder infusion of the starting material. The most important point is that the Si particles evaporate faster in the coupled coil ICTP than in the one-coil ICTP. Therefore, the coupled coil ICTP offers a favorable temperature field for evaporation, while in stable operation, the ICTP remains in the upper area of the plasma torch.

A similar trend can be seen in Figure 16, where variations in particle diameter occur in the ICTP coil along with the twelve turns coil. All particle diameters shrink with time, and the axial position is 220 mm after the start of evaporation. This shrinkage, in turn, implies that the ICTP coupled coil has a favorable temperature field for evaporation. At the same time, for reliable operation, the ICTP stays toward the top of the plasma torch.

Figure 16 shows the radial temperature allocation at z=260 mm. An increase in the feed rate shrinkages the axial temperature of the ICTP. However, the powder level of the raw material hardly affects the temperature beyond the 6 mm radial position. This implies that the Si administration of 0.5 g/min is too heavy to vaporize all the feedstock injected in a one ICTP. High-temperature areas have more internal input power.

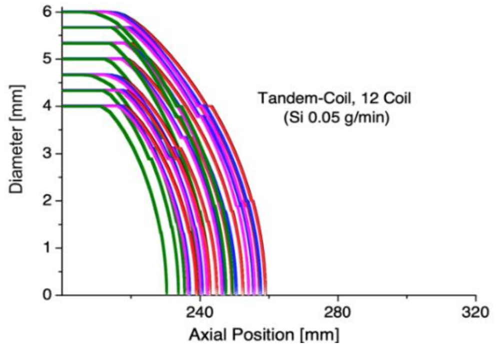

Figure 14. Variation of the diameter of the 35 Si particles in Ar-H_2 coupled-coil ICTP using a 12-turn coil with supplied 0.05 g/min

Figure 15. Variation of the diameter of the 35 Si particles in Ar-H_2 coupled-coil ICTP using a 12-turn coil with supplied 0.01 g/min

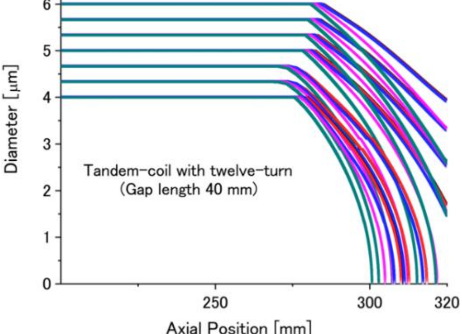

Figure 16. Variation of the diameter of the 35 Si particles in Ar-H2 coupled-coil ICTP using a 12-turn coil with supplied 0.5 g/min

5. CONCLUSION

As described here, the gas flow field and temperature are numerical simulations for the coupled coil ICTP. A lower coil in a plasma torch is formed for nanopowder production, and two upper coils confirm the ICTP coupled coil. The temperature allocation and evaporation of Si powder from the starting material with the coupled-coil ICTP were recorded for the different infusions of the starting material powder between the upper and lower coils and the coil turns. The conclusion showed that the temperature allocation of the ICTP Coupled-coil has increased in the high-temperature range, which can be controlled disjunct on the ICTP Coupled-coil. Meanwhile, with an increasing infusion of Si feed powder, the axial temperature shrinkages because the power consumption for Si feed is evaporation, and the Si feed is more than 0.5 g/min, too heavy to vaporize all injected feed. These results indicate that the ICTP and the twelve-turn coil provide a favorable temperature field for evaporation. Simultaneously, the ICTP remains in the plasma torch's top region for steady operation. This cost-effective temperature range and evaporation are expected to be an ICTP coupled coil advantage over one coil.

REFERENCES

[1] G. Nutsch, “Atmospheric induction plasma spraying,” *High Temperature Material Processes (An International Quarterly of High-Technology Plasma Processes)*, vol. 15, no. 1, pp. 61–74, 2011, doi: 10.1615/HighTempMatProc.v15.i1.80.

[2] K. Shinoda, Y. Kojima, and T. Yoshida, “In situ measurement system for deformation and solidification phenomena of Yttria-stabilized Zirconia droplets impinging on quartz glass substrate under plasma-spraying conditions,” *Journal of Thermal Spray Technology*, vol. 14, no. 4, pp. 511–517, Dec. 2005, doi: 10.1361/105996305X76531.

[3] J. D. Pedersen, H. J. Esposito, and K. S. Teh, “Direct synthesis and characterization of optically transparent conformal zinc oxide nanocrystalline thin films by rapid thermal plasma CVD,” *Nanoscale Research Letters*, vol. 6, no. 1, Dec. 2011, doi: 10.1186/1556-276X-6-568.

[4] J. O. Berghaus, J.-L. Meunier, and F. Gitzhofer, “Monitoring and control of RF thermal plasma diamond deposition via substrate biasing,” *Measurement Science and Technology*, vol. 15, no. 1, pp. 161–164, Jan. 2004, doi: 10.1088/0957-0233/15/1/023.

[5] S. Matsumoto, M. Hino, and T. Kobayashi, “Synthesis of diamond films in a rf induction thermal plasma,” *Applied Physics Letters*, vol. 51, no. 10, pp. 737–739, Sep. 1987, doi: 10.1063/1.98851.

[6] H. Tanaka, T. Osawa, Y. Moriyoshi, M. Kurihara, S. Maruyama, and T. Ishigaki, “Improvement of the anode performance of graphite particles through surface modification in RF thermal plasma,” *Thin Solid Films*, vol. 457, no. 1, pp. 209–216, Jun. 2004, doi: 10.1016/j.tsf.2003.12.024.

[7] Y. Alinejad, N. Faucheux, and G. Soucy, “Preosteoblasts behavior in contact with single-walled carbon nanotubes synthesized by radio frequency induction thermal plasma using various catalysts,” *Journal of Applied Toxicology*, vol. 33, no. 10, pp. 1143–1155, Oct. 2013, doi: 10.1002/jat.2875.

[8] A. Shahverdi and G. Soucy, “Thermogravimetric analysis of single-walled carbon nanotubes synthesized by induction thermal plasma,” *Journal of Thermal Analysis and Calorimetry*, vol. 110, no. 3, pp. 1079–1085, Dec. 2012, doi: 10.1007/s10973-011-2114-4.

[9] S. Choi, J. Matsuo, and T. Watanabe, “Synthesis of AlB 12 and YB 66 nanoparticles by RF thermal plasmas,” *Journal of Physics: Conference Series*, vol. 441, Jun. 2013, doi: 10.1088/1742-6596/441/1/012030.

[10] V. Colombo, E. Ghedini, M. Gherardi, and P. Sanibondi, “Evaluation of precursor evaporation in Si nanoparticle synthesis by inductively coupled thermal plasmas,” *Plasma Sources Science and Technology*, vol. 22, no. 3, May 2013, doi: 10.1088/0963-0252/22/3/035010.

[11] V. Colombo, E. Ghedini, M. Gherardi, and P. Sanibondi, “Modelling for the optimization of the reaction chamber in silicon nanoparticle synthesis by a radio-frequency induction thermal plasma,” *Plasma Sources Science and Technology*, vol. 21, no. 5, Oct. 2012, doi: 10.1088/0963-0252/21/5/055007.

[12] R. Pristavita, N.-Y. Mendoza-Gonzalez, J.-L. Meunier, and D. Berk, “Carbon nanoparticle production by inductively coupled thermal plasmas: controlling the thermal history of particle nucleation,” *Plasma Chemistry and Plasma Processing*, vol. 31, no. 6, pp. 851–866, Dec. 2011, doi: 10.1007/s11090-011-9319-y.

[13] M. Shigeta and T. Watanabe, “Growth model of binary alloy nanopowders for thermal plasma synthesis,” *Journal of Applied Physics*, vol. 108, no. 4, Aug. 2010, doi: 10.1063/1.3464228.

[14] J.-G. Li, M. Ikeda, R. Ye, Y. Moriyoshi, and T. Ishigaki, “Control of particle size and phase formation of TiO_2 nanoparticles synthesized in RF induction plasma,” *Journal of Physics D: Applied Physics*, vol. 40, no. 8, pp. 2348–2353, Apr. 2007, doi: 10.1088/0022-3727/40/8/S14.

[15] J. Szépvölgyi *et al.*, “Effects of precursors and plasma parameters on fullerene synthesis in RF thermal plasma reactor,” *Plasma Chemistry and Plasma Processing*, vol. 26, no. 6, pp. 597–608, Dec. 2006, doi: 10.1007/s11090-006-9036-0.

[16] C. Wang *et al.*, “Effect of ambient gas and pressure on fullerene synthesis in induction thermal plasma,” *Thin Solid Films*, vol. 425, no. 1–2, pp. 41–48, Feb. 2003, doi: 10.1016/S0040-6090(02)01128-8.

[17] Y. Siregar, Y. Nakano, Y. Tanaka, Y. Uesugi, and T. Ishijima, “Numerical study of temperature and gas flow fields in Ar-O_2 tandem-type inductively coupled thermal plasma with Ti feedstock powder injection,” *Journal of Physics D: Applied Physics*, vol. 52, no. 41, Oct. 2019, doi: 10.1088/1361-6463/ab314e.

[18] S. Kolev, A. Shivarova, K. Tarnev, and T. Tsankov, “2D fluid-plasma model of a tandem-type plasma source,” *Journal of Physics: Conference Series*, vol. 113, May 2008, doi: 10.1088/1742-6596/113/1/012011.

[19] W. Li, R. Yang, J. Zheng, and X. Li, “Tandem plasma reactions for Sn/C composites with tunable structure and high reversible lithium storage capacity,” *Nano Energy*, vol. 2, no. 6, pp. 1314–1321, Nov. 2013, doi: 10.1016/j.nanoen.2013.06.012.

[20] Y. Siregar, Y. Tanaka, Y. Uesugi, and T. Ishijima, “Numerical parametric investigation on the temperature distribution in Ar-O_2 induction thermal plasmas with Ti powder injection: Inclusion of particle evaporation,” *IEEJ Transactions on Electrical and Electronic Engineering*, vol. 15, no. 1, pp. 12–23, Jan. 2020, doi: 10.1002/tee.23022.

[21] Y. Siregar, Y. Tanaka, Y. Uesugi, and T. Ishijima, “Influence of input power in Ar-H_2 thermal plasma with silicon powder by numerical simulation,” *Telecommunication Computing Electronics and Control (TELKOMNIKA)*, vol. 17, no. 2, Apr. 2019, doi: 10.12928/telkomnika.v17i2.10533.

[22] Y. Siregar, N. Kodama, Y. Tanaka, T. Ishijima, and Y. Uesugi, "Numerical simulation on thermal plasma temperature field in the torch for different conditions," *IOP Conference Series: Materials Science and Engineering*, vol. 309, Feb. 2018, doi: 10.1088/1757-899X/309/1/012090.
[23] Y. Siregar, Y. Tanaka, T. Ishijima, and Y. Uesugi, "Influence of sheath gas flow rate in Ar induction thermal plasma with Ti powder injection on the plasma temperature by numerical calculation," *MATEC Web of Conferences*, vol. 218, Oct. 2018, doi: 10.1051/matecconf/201821804030.
[24] Y. Takeuchi, Y. Tanaka, Y. Uesugi, S. Kaneko, and S. Okabe, "Numerical simulation of thermal interaction between polymer and argon induction thermal plasma," *Electronics and Communications in Japan*, vol. 92, no. 1, pp. 24–33, Jan. 2009, doi: 10.1002/ecj.10226.
[25] D. Wang, K. Lu, and P. O. Rasmussen, "High-frequency signal injection method based on duty cycle shifting without maximum fundamental voltage magnitude loss," *IEEE Journal of Emerging and Selected Topics in Power Electronics*, vol. 5, no. 3, pp. 1225–1236, Sep. 2017, doi: 10.1109/JESTPE.2017.2690398.
[26] C. T. Crowe, M. P. Sharma, and D. E. Stock, "The particle-source-in cell (PSI-CELL) model for gas-droplet flows," *Journal of Fluids Engineering*, vol. 99, no. 2, pp. 325–332, Jun. 1977, doi: 10.1115/1.3448756.
[27] P. Proulx, J. Mostaghimi, and M. I. Boulos, "Plasma-particle interaction effects in induction plasma modeling under dense loading conditions," *International Journal of Heat and Mass Transfer*, vol. 28, no. 7, pp. 1327–1336, Jul. 1985, doi: 10.1016/0017-9310(85)90163-2.
[28] P. Proulx, J. Mostaghimi, and M. I. Boulos, "Heating of powders in an r.f. inductively coupled plasma under dense loading conditions," *Plasma Chemistry and Plasma Processing*, vol. 7, no. 1, pp. 29–52, Mar. 1987, doi: 10.1007/BF01015998.
[29] P. Fauchais and A. Vardelle, "Thermal plasmas," *IEEE Transactions on Plasma Science*, vol. 25, no. 6, pp. 1258–1280, 1997, doi: 10.1109/27.650901.
[30] W. F. Luder, "Tables of thermodynamic and transport properties of air, argon, carbon dioxide, carbon monoxide, hydrogen, nitrogen, oxygen and steam (Hilsenrath, Joseph)," *Journal of Chemical Education*, vol. 38, no. 10, Oct. 1961, doi: 10.1021/ed038p536.3.
[31] E. J. Rosenboum, "The mathematical theory of non-uniform gases (Chapman, S.; Cowling, T. G.)," *Journal of Chemical Education*, vol. 18, no. 1, Jan. 1941, doi: 10.1021/ed018p48.2.

BIOGRAPHIES OF AUTHORS

Yulianta Siregar was born July 09, 1978 in Medan, North Sumatera Utara, Indonesia. He did his undergraduate work at University of Sumatera Utara in Medan, North Sumatera Utara, Indonesia. He received a Bachelor of Electrical Engineering in 2004. After a while, he worked for a private company. He continued taking a master's program in Electrical Engineering at the Institute of Sepuluh Nopember, Surabaya, West Java, Indonesia, from 2007-2009. He was in a Ph.D. program at Kanazawa University, Japan, from 2016-2019. Until now, he lectured at Universitas Sumatera Utara. He can be contacted at email: julianta_srg@usu.ac.id.

Yasunori Tanaka received B.S., M.S., and Ph.D. degrees in electrical engineering from Nagoya University in 1993, 1995, and 1998, respectively. In April 1998, he was appointed a Research Associate at Kanazawa University. He has been a Professor since August 2010. His research interests include arc interruption phenomena and thermal plasma applications. Prof. Tanaka is a member of Plasma and Fusion Research and the Japan Society of Applied Physics. He can be contacted at email: tanaka@ec.t.kanazawa-u.ac.jp.